Sustainable Solutions in Structural Engineering and Construction
Edited by Chantawarangul, K., Suanpaga, W., Yazdani, S., Vimonsatit, V., and Singh, A.

ISBN: 978-0-9960437-0-0

GROUND DISPLACEMENT BEHAVIORS CONSIDERING UNSTEADY SEEPAGE FLOW AND NON-LINEAR DEFORMATION

HARUYUKI YAMAMOTO and LINGYU MENG

Development Technology, Hiroshima University/IDEC, Hiroshima, Japan

One major concern for excavation projects is the ground displacement generated around the excavated zone. In this paper, a 2-dimensional model analysis was made on non-linear ground behavior around excavation due to unsteady seepage of groundwater, taking into account the saturated-unsaturated theory by using Toyo-ura sand. The finite-element method and finite-different method were employed to study the space problem and time dimension, respectively. The numerical simulation code implemented by FORTRAN was applied to predict the flow-velocity distribution and the results of ground displacement. To validate the programming, a simple model was tested for comparison with tri-axial test data. The samples were made of Toyo-ura sand with a relative density of 90%. The programming also calculated flow-velocity distribution and ground displacement results of dewatering in excavation work over time. Results showed that the effect of horizontal displacement caused by seepage flow plays a very important role in the displacement field. This numerical simulation method provides a more reasonable computing scheme compared to traditional methods. All have theoretical meaning and applicable value, and also present useful references for the excavation stability and disaster prediction.

Keywords: Excavation projects, Seepage force, Non-linear analysis, Numerical simulation.

1 INTRODUCTION

Excavation has been one of the most common engineering works in ancient construction as well as in today's civil engineering projects. One of the major concerns for many excavation projects is the ground displacement generated around the excavated zone. In recent years, with the rapid development of computer technology and the finite-element method (FEM), ground behavior due to the seepage flow of groundwater has been emphasized more heavily (Debidin 1980, Holt 1992, Hsi 1992). In this paper, a 2-dimensional model analysis was made on the non-linear ground behavior around the excavation due to unsteady seepage of groundwater, taking into account the saturated-unsaturated theory by using Toyo-ura sand.

2 ANALYTICAL THEORIES AND BACKGROUND

Figure 1 shows the elevation of the excavation, where EB is the width and EH is the depth of the excavation area. In this analysis, half of the area has been selected as the analytical area because of symmetry, shown in Figure 2. This model has the following

basic assumptions: The ground water flow is laminar and governed by Darcy's law. The water molecules and soil particles cannot be compressed. The stress-strain relationship of the soil is ruled by the Duncan-Chang model (Duncan 1970). The coefficient of permeability variation in the unsaturated region obeys the Van-Genuchten model (Van Genuchten 1980), while remaining unchanged within the saturated region. Table 1 shows the material coefficients of the V-G model for Toyo-ura sand (Kiyohara 2007), and Table 2 the material parameters of the D-C model for Toyo-ura sand (Sun 1998).

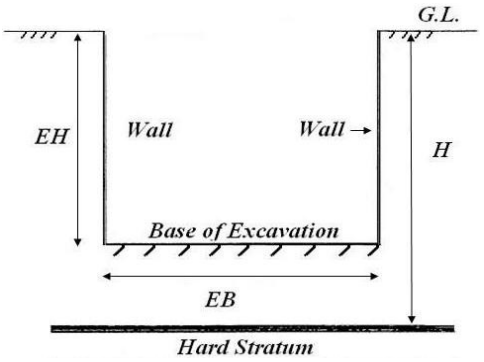

Figure 1. Elevation of excavation.

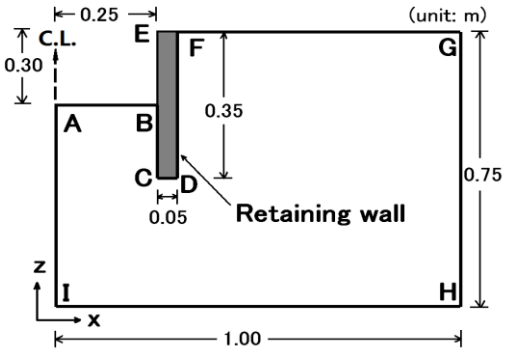

Figure 2. FEM analytical area.

Table 1. Material constants for V-G model.

Ksat (cm/s)	α	θs	θr	n
0.025	5.52	0.41	0.00	12.96

Table 2. Material constants for D-C model.

K	Rf	υ	Φ	n	c
397	0.9	0.3	41°	0.7	0

2.1 Seepage Analysis

Considering Darcy's law, the differential equation governing flow through porous media (Nishigaki 2010) is:

$$\frac{\partial}{\partial x}\left(K_x \frac{\partial h}{\partial x}\right)+\frac{\partial}{\partial y}\left(K_y \frac{\partial h}{\partial y}\right)+\frac{\partial}{\partial z}\left(K_z \frac{\partial h}{\partial z}\right)+Q=(\ \beta S_S+Cs)\frac{dh}{dt} \tag{1}$$

where Kx, Ky, Kz are coefficients of permeability in x, y, z directions, h is the total head, Q is drainage volume, Ss is specific storage, and Cs is specific capacity. β = 1 (saturated situation), and β = 0 (unsaturated situation). The finite-element equation is obtained through the variational procedure of Eq. (1) as:

$$[H]\{h\}+[C]\left\{\frac{dh}{dt}\right\}=0 \tag{2}$$

where [H] is the seepage matrix and [C] is the capacity matrix. Based on the FDM, Eq. (2) can be transformed into Eq. (3). In Eq. (3), for calculating the value of $[H_{ij}]^{k+1}$ and $[C_{ij}]^{k+1}$, a presumption of $\{h_j\}^{k+1}$ should be made. $\{h_j\}^{k+1/2}$ is used to calculate $[H_{ij}]^{k+1/2}$

and $[C_{ij}]^{k+1/2}$, which can approximately replace the $[H_{ij}]^{k+1}$, $[C_{ij}]^{k+1}$ and $[C_{ij}]^{k}$, here, k is the time step, Δt is the time increment, ω ($\omega = 0.5$) is the weight parameter.

$$(1-\omega)\left[H_{ij}\right]^{k}\left\{h_j\right\}^{k}+\omega\left[H_{ij}\right]^{k+1}\left\{h_j\right\}^{k+1}+\frac{1}{\Delta t}\left(\left[C_{ij}\right]^{k+1}\left\{h_j\right\}^{k+1}-\left[C_{ij}\right]^{k}\left\{h_j\right\}^{k}\right)=0 \tag{3}$$

2.2 Displacement Analysis

According to the principle of virtual work for ground displacement, Eq. (4) is obtained in the following form:

$$\int_V \lfloor\delta\varepsilon\rfloor\{\Delta\sigma\}\,dV=\int_S \lfloor\delta u\rfloor\{\Delta T\}\,dS+\int_V \lfloor\delta u\rfloor\{\Delta B\}\,dV+\int_V \lfloor\delta u\rfloor\{\Delta S\}\,dV+\int_L \lfloor\delta u\rfloor\{\Delta P\}\,dL \tag{4}$$

where $\{\Delta P\}$ is the vector concerning point load, $\{\Delta B\}$ is the vector concerning body force, $\{\Delta T\}$ is the vector concerning traction and $\{\Delta S\}$ is the vector concerning seepage force. The matrix form of Eq. (4) can be written as below:

$$[K]\{\Delta U\}=\{\Delta F\} \tag{5}$$

where [K] is the global stiffness matrix, $\{\Delta U\}$ is the global nodal increment displacement vector, and $\{\Delta F\}$ is the global nodal increment force vector.

3 NUMERICAL PREDICTION AND EXPERIMENTAL DATA

To validate the correctness of the programming, a simple model has been tested for comparison with the tri-axial test data. The sample was made of Toyo-ura sand with a relative density of 90%, as implemented by Yamamoto (1991). The confining pressure varies from 50 KPa, 100 KPa, 150 KPa, 200 KPa, 250 KPa to 300 KPa. Loading is acted on the specimen until failure. Figure 3 shows the comparison of numerical predictions and experimental data under loading conditions with different confining pressures. Numerical prediction results matched well with the tri-axial test data, which ensures the programming is valid. The influence of the soil resilience of deep pit excavation's bottom due to dewatering is inevitable during the excavation. Therefore, it is necessary to consider the unloading phenomenon when numerical prediction is implemented.

Figure 4 shows the comparison of numerical prediction results and tri-axial test data under unloading-reloading condition with confining pressure equal to 100 Kpa. Comparing the prediction results with the tri-axial test, the numerical prediction results matched well with the test data, confirming the correctness of the analysis programming under unloading-reloading condition.

4 NUMERICAL PREDICTIONS FOR THE MODEL

The size of the model was 2 m $\times$ 0.75 m, the excavation site 0.5 m $\times$ 0.2 m, and the retaining wall 0.05 m $\times$ 0.35 m. Half of the area was selected for analysis to save computing time and storage space, as shown in Figure 2. The material constants of V-G and D-C are from Table 1 and Table 2, respectively. Boundary conditions for the seepage flow are given as below:

- On AB: total head H = 0.55 m; on GH: total head H = 0.75m.

Boundary conditions for the displacement are given as below:

- On AI, BC, FD and GH: the displacement in X direction has been fixed; on IH: the displacement in Z direction has been fixed.

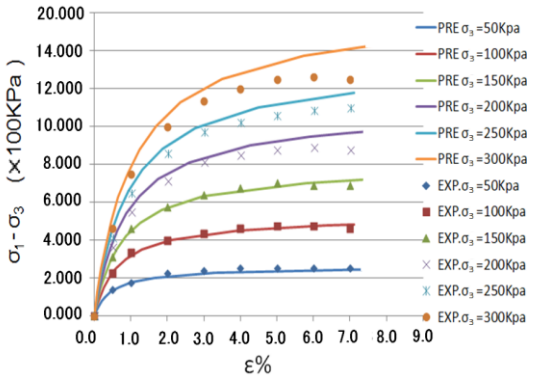

Figure 3. Comparison of numerical prediction and experimental data under loading condition.

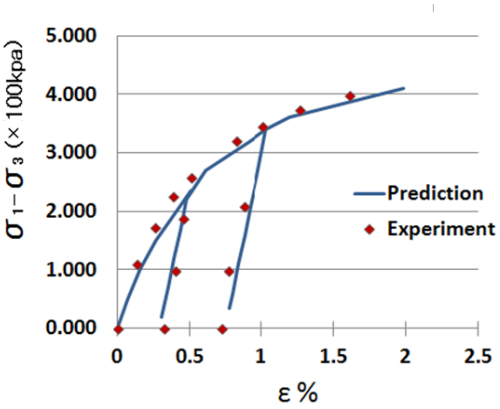

Figure 4. Comparison of numerical prediction results and tri-axial test data under unloading-reloading condition.

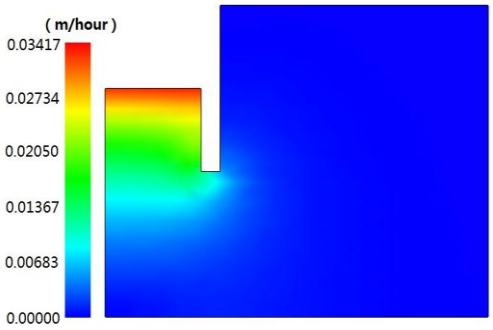

Figure 5. Composite flow velocity distribution T = 36sec.

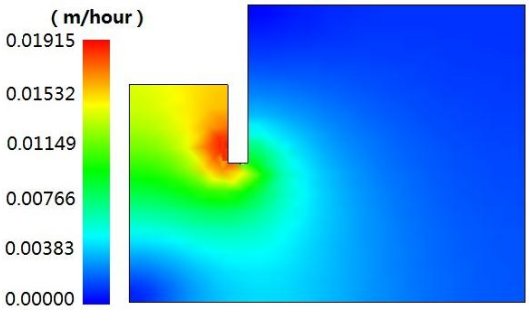

Figure 6. Composite flow velocity distribution T = 180 sec.

The calculated results of seepage flow are shown in Figures 5, 6 and 7 at different points in time. When time equaled 360sec, the seepage became an almost steady flow. The maximum velocity zone appeared around the bottom of the excavation at an early stage (T = 36sec). The peak value of composite velocity near the excavation bottom was almost 0.035 m/hour (Figure 5), and after that the velocity decreased gradually over time (Figures 6 and 7). When T = 36sec, the seepage was an unsteady flow, the affected area of seepage was not full-area, and the seepage flow behind the retaining wall was nearly zero. Over time, the affected area of seepage became progressively larger, as shown in Figure 6 (T = 180sec).

The seepage flow became nearly steady when T = 360 sec, as shown in Figure 7. The high-velocity zone mainly appeared around the bottom of the excavation at early stage, as shown in Figure 5. Over time, the seepage velocity around the bottom began to decrease until it was reduced by half. The high-velocity zone came from the corner of the retaining wall (around point C in Figure 2), as shown in Figure 7.

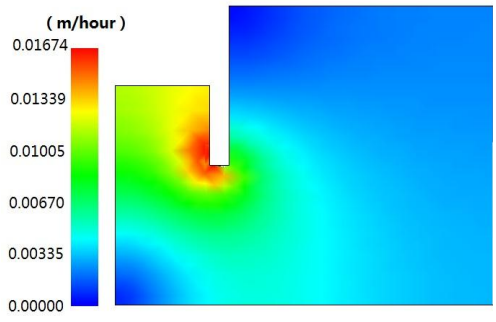

Figure 7. Composite flow velocity distribution T = 360 sec.

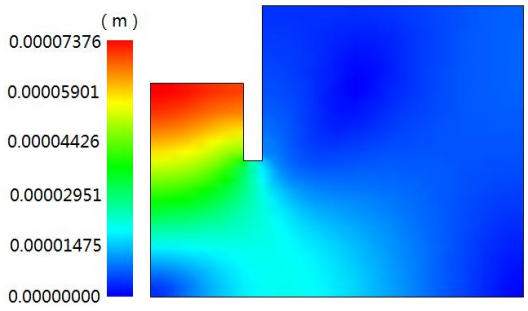

Figure 8. Composite displacement distribution T = 36sec.

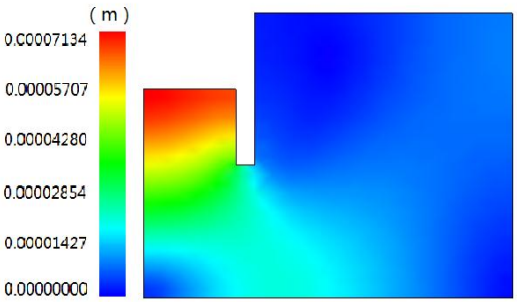

Figure 9. Composite displacement distribution T = 180 sec.

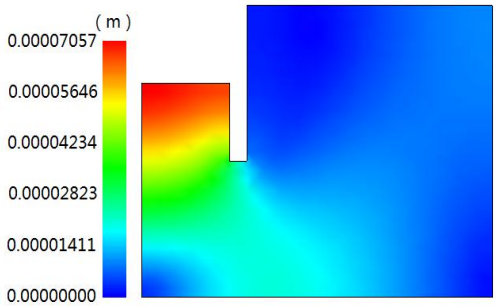

Figure 10. Composite displacement distribution T = 360 sec.

The calculated results of composite displacement are shown at different points in time in Figure 8 (T = 36 sec), Figure 9 (T = 180 sec), and Figure 10 (T = 360sec). The maximum vertical displacement zone appears at the bottom of the pit at all times. The peak value of displacement at the excavation bottom is almost 0.000074 m in Figure 8, and decreases slightly over time as shown in Figures 9 and 10. This is because the seepage velocity under the bottom of the pit was relatively larger during the initial period of unsteady seepage flow, which can lead to a larger seepage force, and cause relatively larger vertical displacement. Compared with the early stage (T = 36 sec), the final displacement (T = 360 sec) only decreases by 5% when the seepage flow is reduced by half. This is because the D-C model is a nonlinear-elastic model, meaning the modulus for loading and the modulus for unloading is different, which can describe the elasto-plasticity of soil approximately. A relatively larger horizontal-displacement region appeared above the hard stratum at all times, mainly due to the horizontal seepage flow. The large vertical-displacement region under the bottom of the pit is due

to the vertical-seepage flow. The large-displacement zones gradually create a spoon-shaped zone behind the retaining wall when enough time passes, as shown in Figure 10.

5 CONCLUSIONS

In this paper, a numerical model test was performed on ground behavior around an excavation due to unsteady seepage of groundwater using a proposed FEM-FDM program. The numerical prediction showed that the vertical upward seepage velocity below the bottom of the pit is relatively larger at the early stage of the seepage field and decreases gradually over time. The maximum velocity zone appears at the foot of the excavation at an early stage where the potential seepage failure, such as quicksand and piping, could happen. The maximum displacement zone appeared at the bottom of the pit and extends gradually over time, which matched well with the results of the seepage field. Displacement caused by the seepage flow plays a very important role in the displacement field, and a 2D sliding surface may appear after enough time, indicating that a seepage-force numerical analysis is necessary to present a useful reference to excavation stability and disaster prediction.

References

Debidin, F., and Lee. C. F., Groundwater and drawdown in a large earth excavation, *National Research Council of Canada*, 17(2), 185-202, May, 1980.

Duncan, J. M. et al., Nonlinear analysis of stress and strain in soils, *Proc. ASCE*, SM5, 1629-53, 1970.

Holt, D. A., and Griffiths. D. V., Transient analysis of excavations in soil, *Computer and Geotechnics*, 13, 159-74, 1992.

Hsi, J. P., and Small. J. C., Analysis of excavation in an elasto-plastic soil involving drawdown of the water table, *Computer and Geotechnics*, 13, 1-19, 1992.

Kiyohara, Y. et al, The applicability of Hachinohe *shirasu* as material of capillary barrier, *Japanese Geotechnical Journal*, 329-37, 2007 (in Japanese).

Nishigaki, M., *Simulation of Groundwater Flow and Solute Transport*, Gihodo Press, Japan, 34-55, 2010 (in Japanese).

Sun, D. A., Estimate of initial modulus of hyperbolic stress-strain relation from result of consolidation tests, *Thirteenth Southeast Asian Geotechnical Conference*, 171-6, 1998.

Van Genuchten. M. T. H., A Closed-form equation for predicting the hydraulic conductivity of unsaturated soils, *Soil Sci. Soc*, 892-8, 1980.

Yamamoto, H., Model tests of friction piles in sand by means of the hydraulic gradient similarity method, *Journal of Structural Engineering*, Vol. 37B, 11-22, 1991 (in Japanese).